PREDICTION OF FORMING LIMIT OF HIGH-STRENGTH STEEL SHEETS

Hirohiko Takuda, Hitoshi Fujimoto, Takayuki Hama, Toshinori Maruyama –
Kyoto University, Japan

ABSTRACT

In this study, first, the possibility of the application of some criteria for ductile fracture to the high-strength steel sheets is examined. The forming limits of a few types of high-strength steel sheets under various strain paths from balanced biaxial to uniaxial tension are examined by the Marciniak-type in-plane biaxial stretching test, and they are compared with those derived from the ductile fracture criteria. As a result, it turns out that the fracture strains derived from the criterion by Cockcroft and Latham give the best fit to the experimental results. Next, as fundamental 3-dimensional press forming processes, square cup deep drawing and T-shape forming of high-strength steel sheets are analysed by the finite element method combined with the ductile fracture criterion. The dynamic explicit finite element program LS-DYNA with membrane shell is used. The comparison with the experimental results demonstrates that the fracture initiation site and the critical punch stroke are successfully predicted by the present approach.

KEYWORDS

Forming limit, ductile fracture criterion, sheet forming process, 3-dimensional finite element simulation, square cup deep drawing, T-shape forming

INTRODUCTION

The use of high-strength steel sheets to reduce car weight is drawing much attention from the viewpoint of environmental preservation. However, high-strength steel sheets are much inferior to ordinary steel sheets in formability. Due to the less formability the forming limit prediction in very important to find the forming method and conditions suitable for the high-strength steel sheets.

In sheet metal forming, the forming limit is generally determined by the onset of localized necking and predicted by the tensile instability or bifurcation theories. However, the conventional approaches are not always suitable, depending on the sheet materials. The authors have recently proposed an approach to predict the forming limit by introducing criteria for ductile fracture into the finite element simulation of sheet metal forming processes [1-4]. In this approach the forming limit is predicted not by the onset of localized necking, but by the occurrence of fracture itself. In the criteria the occurrence of ductile fracture is estimated by the macroscopic stress and strain during forming, which are calculated by the finite element simulation.

In this study, the possibility of the prediction of the forming limit of high-strength steel sheets by means of ductile fracture criteria is examined for some criteria. Fundamental 3-dimensional press forming processes, square cup deep drawing and T-shape forming, of high strength steel sheets are simulated by the finite element program LS-DYNA, and the numerical results are compared with the experimental ones.

HOME

1. MATERIALS

Materials used in this study are a mild steel sheet (A) and two types of high-strength steel sheets (B and C) with a thickness of 1.2 mm. They are expressed as materials A, B and C, respectively, in the later description.

The uniaxial tension tests were carried out in the directions of 0, 45 and 90° to rolling. Fig. 1 shows the true stress-strain curves obtained from the tests in the rolling direction. Table 1 indicates the tensile properties with the average values for the three directions. Here, the true stress-strain relation is approximated by

$$\bar{\sigma} = K\bar{\varepsilon}^{n} \tag{1}$$

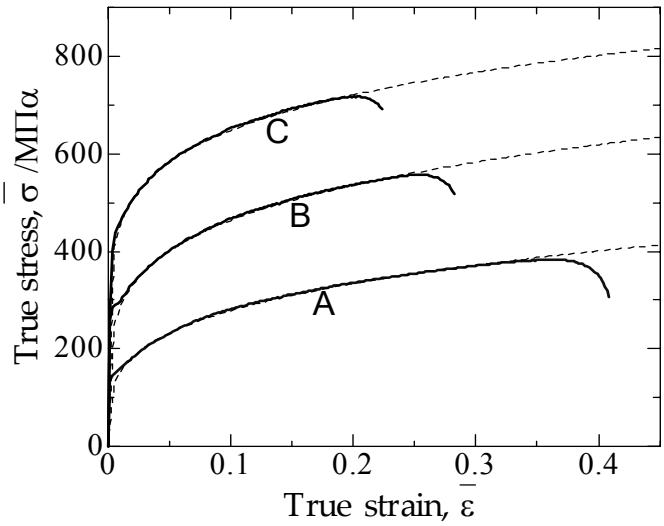

Fig.1 Flow curves in uniaxial tension tests of materials A, B and C. Note that the dotted lines indicate the curves approximated by Eq. 1.

Table 1 Tensile properties of the sheets.

Material	A	B	C
K-value [MPa]	514	750	930
Work-hardening exponent, *n*	0.26	0.21	0.15
Normal anisotropy parameter, *r*	2.12	1.50	1.03
Elongation [%]	51	34	26
Tensile strength [MPa]	280	440	593

2. DUCTILE FRACTURE CRITERIA

Based on various hypotheses many criteria for ductile fracture have been proposed. Among them, the following criteria are examined in this study. In these criteria, the histories of stress and strain affecting the occurrence of the ductile fracture are considered in simple forms, and they can be introduced in the 3-dimensional finite element simulation.

$$\int_0^{\bar{\varepsilon}_f} \sigma_{\max} d\bar{\varepsilon} = C_1 \qquad \text{(Cockcroft and Latham [5])} \qquad (2)$$

$$\int_0^{\bar{\varepsilon}_f} \frac{2}{3}\left(1-\frac{\sigma_h}{\sigma_{\max}}\right)^{-1} d\bar{\varepsilon} = C_2 \qquad \text{(Brozzo et al. [6])} \qquad (3)$$

$$\int_0^{\bar{\varepsilon}_f} \left(\frac{\sigma_h}{\bar{\sigma}} + C_3\right) d\bar{\varepsilon} = C_4 \qquad \text{(Oyane et al. [7])} \qquad (4)$$

$$\int_0^{\bar{\varepsilon}_f} \bar{\sigma} d\bar{\varepsilon} = C_5 \qquad \text{(Clift et al. [8])} \qquad (5)$$

where $\bar{\varepsilon}_f$ is the equivalent strain at which the fracture occurs, $\sigma_{\max}$ is the maximum normal stress, σ_h is the hydrostatic stress, $\bar{\sigma}$ the equivalent stress, $\bar{\varepsilon}$ the equivalent strain, and C_1, C_2, C_3, C_4 and C_5 are material constants.

3. LIMIT STRAINS IN BIAXIAL STRETCHING

For the materials A, B and C the Marciniak-type in-plane biaxial stretching test [9] was carried out. The limit strains for fracture were measured under various strain paths from balanced biaxial stretching to uniaxial tension. The open marks in Fig. 2 show the limit strains measured just at the fracture sites. They are linearly distributed for all the sheets, while the inclination decreases with increase in the tensile strength. Note that the normal anisotropy parameter, *r*, also decreases with increase in the tensile strength (Table 1).

The limit strains in biaxial stretching can be derived from the criteria for ductile fracture. Hill's yield criterion for anisotropic materials [10] is expressed as:

$$F(\sigma_y-\sigma_z)^2 + G(\sigma_z-\sigma_x)^2 + H(\sigma_x-\sigma_y)^2 + 2L\tau_{yz}^2 + 2M\tau_{zx}^2 + 2N\tau_{xy}^2 = \frac{2}{3}(F+G+H)\bar{\sigma}^2 \qquad (6)$$

where F, G, H, L, M and N are anisotropy parameters. When no planer anisotropy is assumed in Eq. (6), the terms in Eqs. (2) to (5) are expressed for the biaxial stretching state by the functions of the normal anisotropy parameter, *r*, and the strain ratio, β (= $\varepsilon_1/\varepsilon_2$, where ε_1 and ε_2 are the major and the minor strains in the plane of a sheet). Provided that the strain ratios are constant during the biaxial stretching until the fracture initiation, the limit strains are simply calculated by the ductile fracture criteria as:

(Cockcroft and Latham):

$$\varepsilon_{1f}=\sqrt{\frac{3(1+2r)^2}{2(2+r)\left\{r(1-\beta)^2+(\beta r+\beta+r)^2+(\beta r+r+1)^2\right\}}}\left[\frac{C_1(n+1)}{(\beta r+r+1)K}\sqrt{\frac{3\left\{r(1-\beta)^2+(\beta r+\beta+r)^2+(\beta r+r+1)^2\right\}}{2(2+r)}}\right]^{\frac{1}{n+1}} \quad (7)$$

(Brozzo et al.):

$$\varepsilon_{1f}=\frac{C_2(\beta r-\beta+r+2)}{2(\beta r+r+1)}\sqrt{\frac{3(1+2r)^2}{2(2+r)\left\{r(1-\beta)^2+(\beta r+\beta+r)^2+(\beta r+r+1)^2\right\}}} \quad (8)$$

(Oyane et al.):

$$\varepsilon_{1f}=\frac{C_4}{\frac{2}{9}(\beta+1)(r+2)+C_3\sqrt{\frac{2(2+r)}{3(1+2r)^2}\left\{r(1-\beta)^2+(\beta r+\beta+r)^2+(\beta r+r+1)^2\right\}}} \quad (9)$$

(Clift et al.):

$$\varepsilon_{1f}=\sqrt{\frac{3(1+2r)^2}{2(2+r)\left\{r(1-\beta)^2+(\beta r+\beta+r)^2+(\beta r+r+1)^2\right\}}}\left[\frac{C_5(n+1)}{K}\right]^{\frac{1}{n+1}} \quad (10)$$

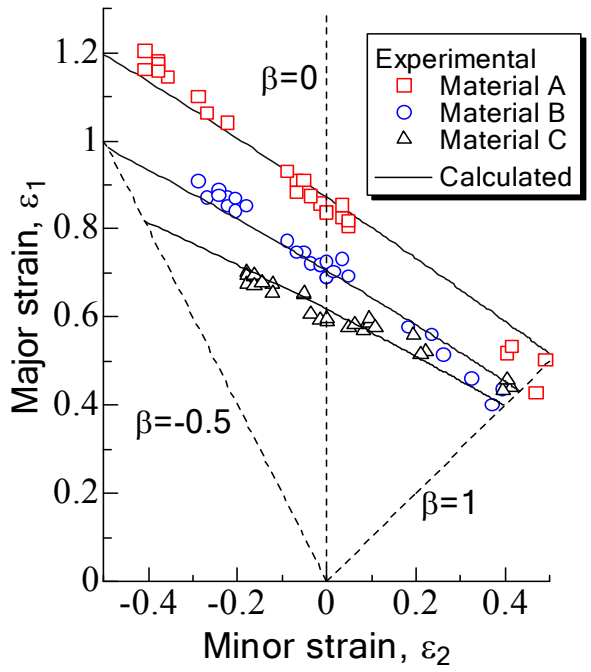

Fig. 2 Limit strains for fracture in biaxial stretching tests.

From the comparison between the limit strains calculated by the above equations and the experimental ones, it is found that the limit strains derived from the criterion by Cockcroft and Latham can give the best fit to the measured ones. Namely, the limit strains calculated by the eq. (7) are distributed linearly and the inclination of the lines decreases with r-value, corresponding to the experimental results. The solid lines in Fig. 2 indicate the limit strains for the three kinds of sheets derived from the criterion by Cockcroft and Latham using the tensile properties shown in Table 1 and the material constant C_1. The material constant C_1 in the criterion is determined as to be 600, 620 and 640 MPa for the materials A, B and C, respectively.

4. FINITE ELEMENT SIMULATION OF SQUARE CUP DEEP DRAWING AND T-SHAPE FORMING TESTS

The square cup deep drawing and the T-shape forming tests were carried out for the above sheets. Fig. 3 shows the dimensions of the tools for the tests. Considering the symmetry, the quarter and the half sections are indicated for the square cup deep drawing and the T-shape forming tests, respectively. Square specimens with a length of 150 mm were used for the deep drawing tests, and two types of rectangular specimens of 200 mm × 120 mm and 200 mm × 160 mm were used for the T-shape forming tests (blue dotted lines in Fig.3). The blank holder force was kept constant at 196 and 19.6 kN at the deep drawing and the T-shape forming tests, respectively. Corrosion resisting oil was used for the lubricant between the specimens and the tools for all the tests.

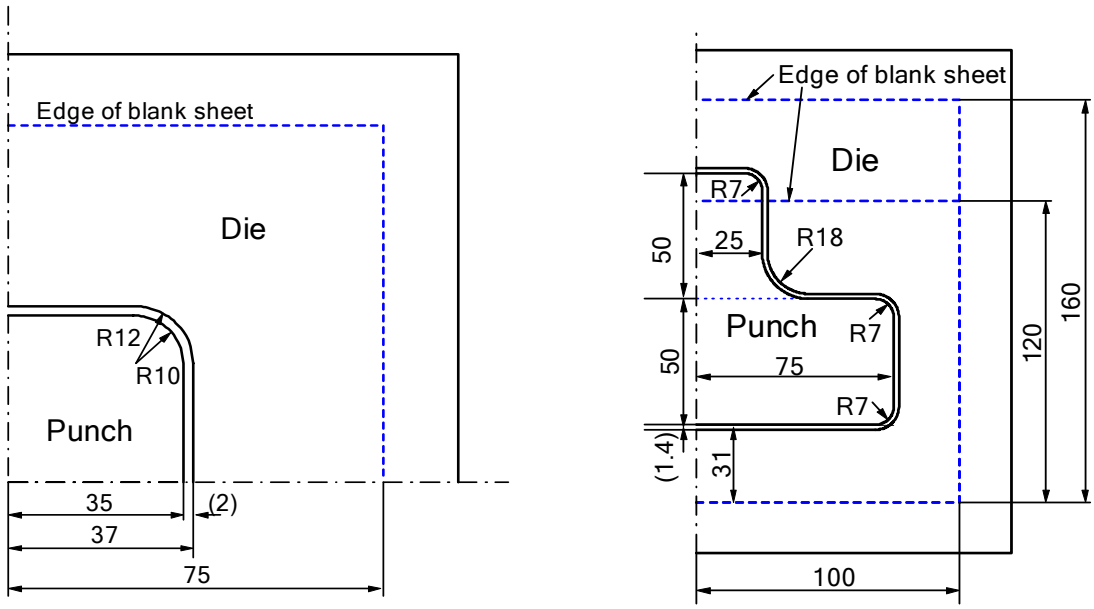

(a) Square cup deep drawing (b) T-shape forming

Fig. 3 Dimensions of tools for square cup deep drawing and T-shape forming.

The above tests are simulated by the explicit finite element program LS-DYNA ver. 970 with 4-node thin shell. The ductile fracture criterion by Cockcroft and Latham is modified and the integral I defined as

$$I = \frac{1}{C_1}\int_0^{\bar{\varepsilon}} \sigma_{\max} d\bar{\varepsilon} \qquad (11)$$

Using the stress and the equivalent strain obtained by the finite element simulation, the integral I is calculated for each element and each deformation step. The condition of fracture is satisfied when and where the integral I amounts to unity. The user-subroutine incorporated in LS-DYNA for the calculation of the integral I is, at present, based on the yield criterion for isotropic materials, i.e. von Mises' yield criterion. Therefore, the forming limit prediction is carried out only for the material C (the high-strength steel sheet of 590 MPa grade). The material C has the r-value of almost 1 (Table 1) and can be considered as isotropic.

5. RESULTS

Since the calculated results greatly depend on the frictional coefficient, μ, the proper value for μ has to be evaluated first. Fig. 4 shows the comparison between the measured punch forces in the T-shape forming tests and those calculated for various values of μ. The punch forces calculated for the coefficient of 0.17 give the best fit to the measured ones. In this figure only the results calculated for the coefficients of 0.14, 0.17 and 0.20 are indicated. Please note that the calculations have been carried out for various coefficients with an interval of 0.01.

The red solid line in Fig. 5 shows the measured profile of the specimen during the T-shape forming test at the punch stroke of 15 mm. The deformed specimen calculated for the frictional coefficient of 0.17 is shaded in this figure. From the comparison between the calculated and the experimental results on the punch force and the specimen profile, it is concluded that the frictional coefficient of 0.17 is suitable for the present simulation. Accordingly, the forming limit prediction described below is carried out using the calculated results for the coefficient of 0.17.

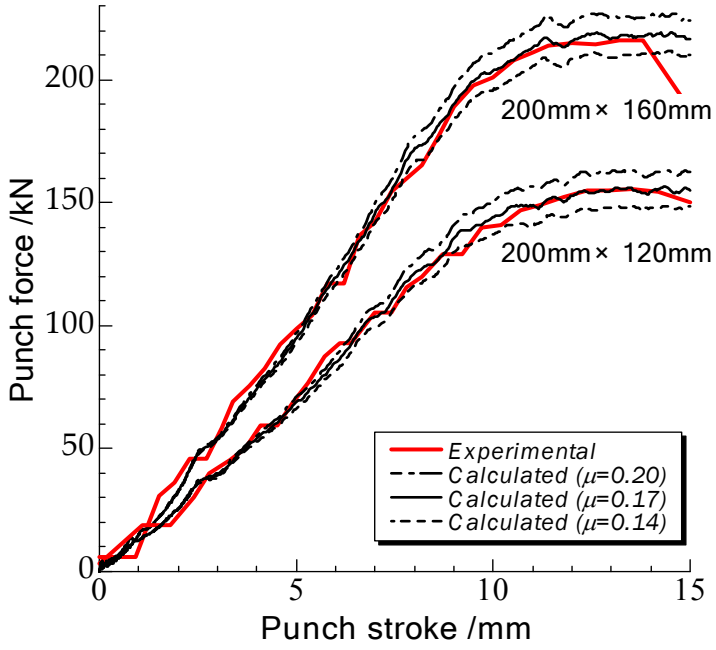

Fig. 4 Comparison between measured punch force and calculated ones for various frictional coefficients, μ.

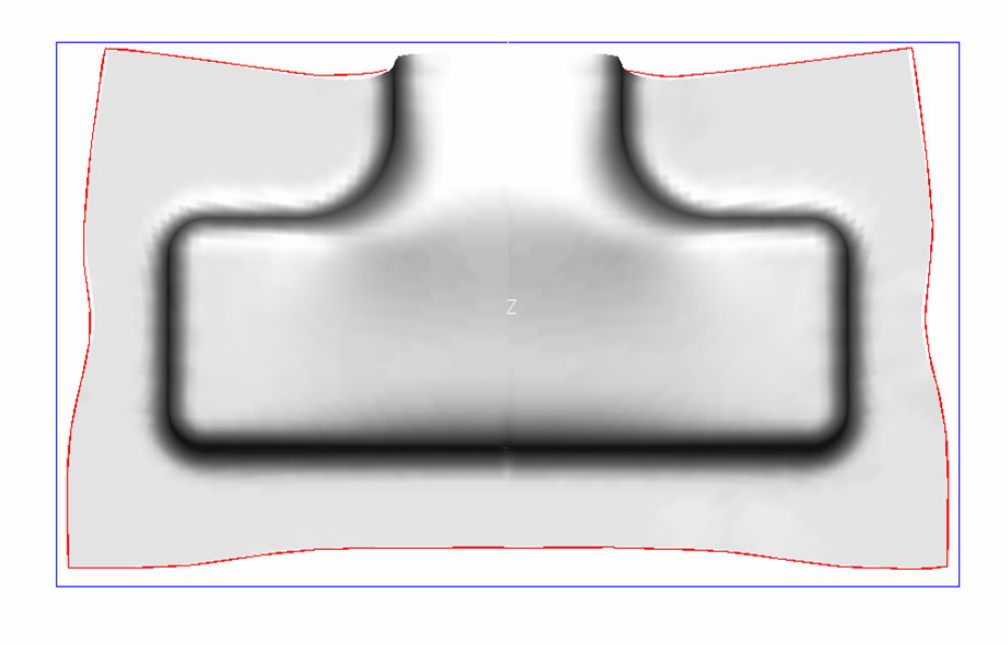

Fig. 5 Blank profile calculated for frictional coefficient of 0.17, in comparison with experimental one drawn with solid line.

Fig. 6 shows the calculated distribution of the integral I at the punch stroke of 26.3 mm in the square cup deep drawing. The integral I at the corner of the punch shoulder amounts to unity, and the fracture initiation at the site (red zone) is predicted. The experimental result for the above case is shown in Fig. 7. It is observed that the fracture occurred at the corner of the punch shoulder. The critical punch stroke at the fracture initiation was measured to be 27.3 mm. Note that the drawing test was stopped at the punch stroke of 30 mm and the specimen shown in this figure was drawn until the punch stroke after the fracture initiation.

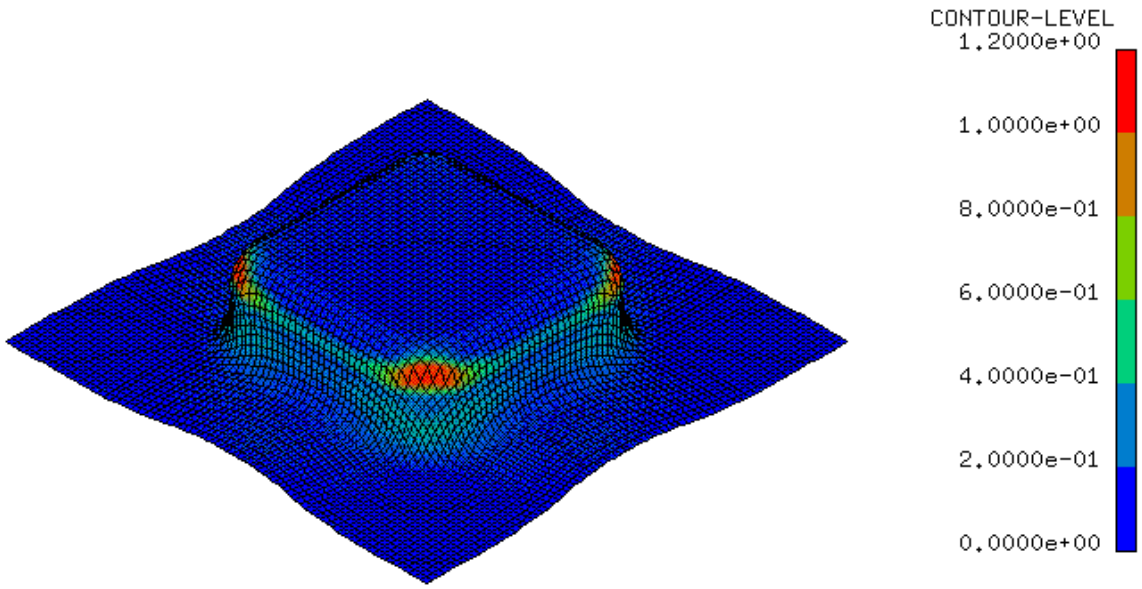

Fig.6 Calculated distribution of the integral I at punch stroke of 26.3 mm in square cup deep drawing.

Fig. 7 Specimen after square cup deep drawing test.

In the T-shape forming tests the fracture initiation sites differ depending on the size of specimen. In case of the specimen of 200 mm × 120 mm the fracture occurred at the corner of the punch shoulder, and in case of 200 mm × 160 mm at the sidewall, as shown in Figs. 8(a) and (b), respectively. And the critical punch strokes were measured to be 17.8 and 13.8 mm, respectively. The calculated results corresponding to the above cases are shown in Figs. 9(a) and (b). It is observed in Fig. 9(a) that the integral I at the corner of the punch shoulder amounts to unity at the punch stroke of 17.9 mm. Fig. 9(b) shows that the integral I at the sidewall amounts to unity at the stroke of 15.9 mm. Two types of fracture initiation sites including the extension of fracture are well predicted by the simulation.

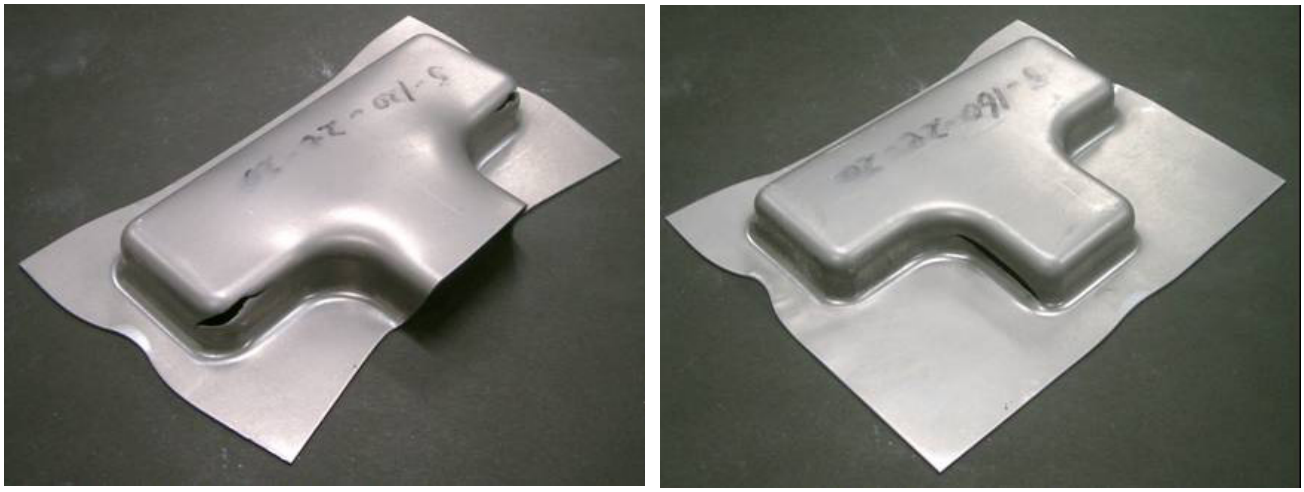

(a) 200mm×120mm (b) 200mm×160mm

Fig. 8 Specimen after T-shape forming test.

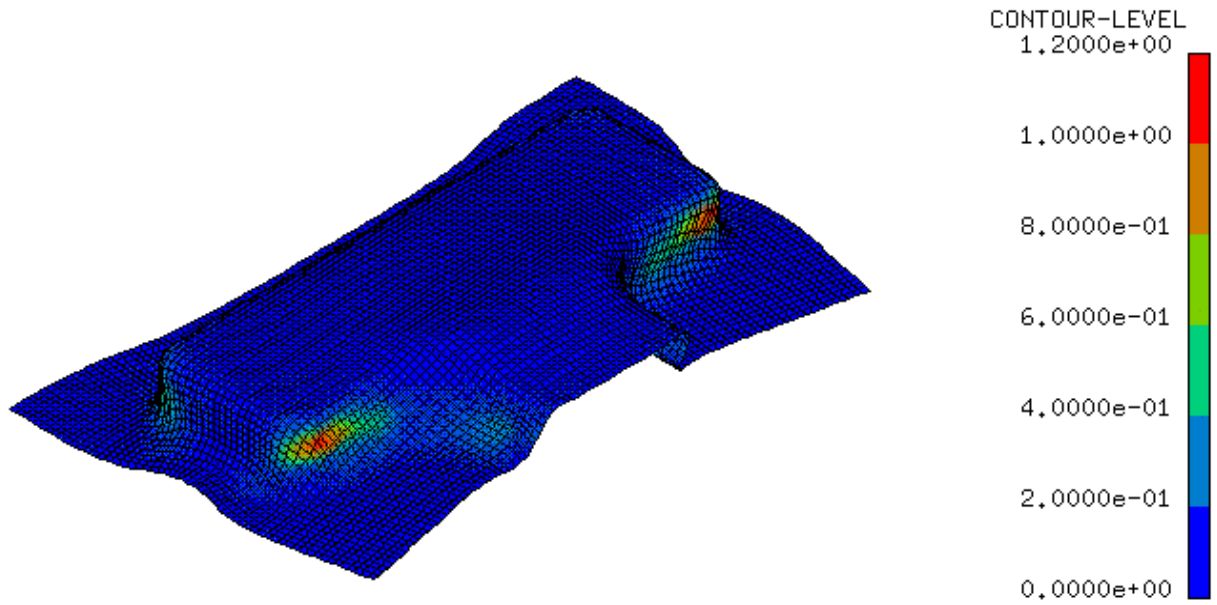

(a) 200mm×120mm, Punch stroke = 17.9mm

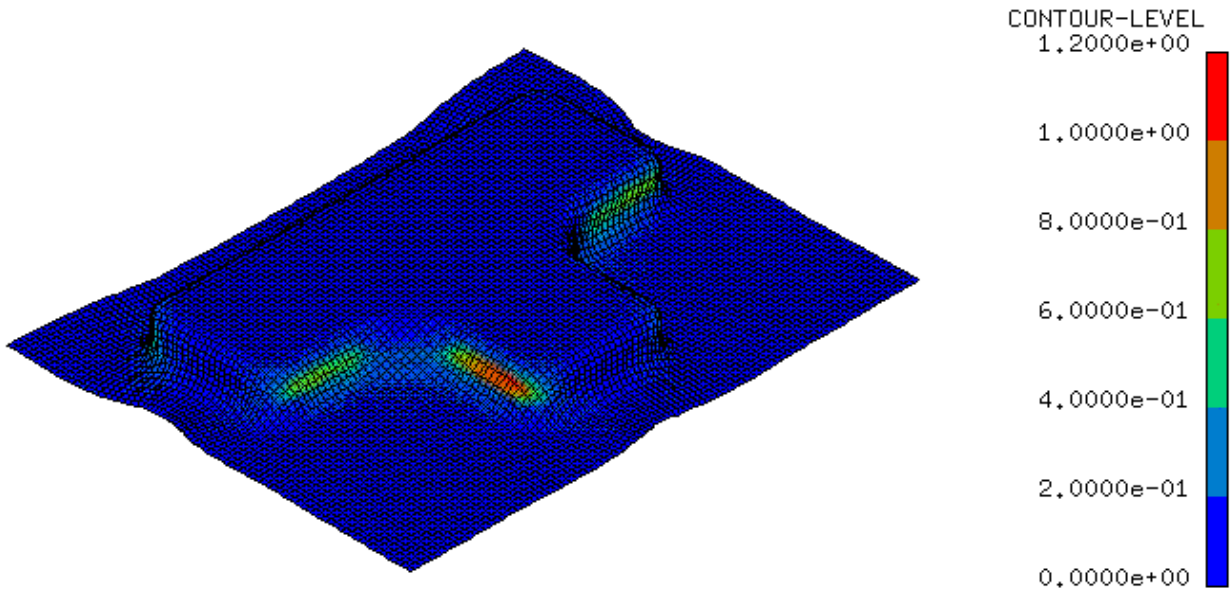

(b) 200mm×160mm, Punch stroke = 15.9mm

Fig. 9 Calculated distribution of the integral *I* in T-shape forming.

It can be concluded that the fracture initiation sites and the critical punch strokes in the three dimensional press forming processes of the high-strength steel sheet are successfully predicted by the finite element simulation combined with the ductile fracture criterion by Cockcroft and Latham.

REFERENCES

1) H. Takuda, K. Mori, H. Fujimoto and N. Hatta, J. Mater. Process. Tech. 60 (1996), p. 291.
2) H. Takuda, K. Mori, H. Fujimoto and N. Hatta, Arch. Appl. Mech. 67 (1997), p. 143.
3) H. Takuda, K. Mori and N. Hatta, J. Mater. Process. Tech. 95 (1999), p. 116.
4) H. Takuda, K. Mori, N. Takakura and K. Yamaguchi, Int. J. Mech. Sci. 42 (2000), p. 785.
5) M.G. Cockcroft and D.J. Latham, J. Inst. Metals 96 (1968), p. 33.
6) P. Brozzo, B. Deluca and R. Rendina, Proc. 7th Biennial Conference of the International Deep Drawing Research Group (1972).
7) M. Oyane, T. Sato, K. Okimoto and S. Shima, J. Mech. Work. Technol. 4 (1980), p. 65.
8) S.E. Clift, P. Hartley, C.E.N. Sturgess and G.W. Rowe, Int. J. Mech. Sci. 32 (1990), p. 1.
9) Z. Marciniak and K. Kuczynski, Int. J. Mech. Sci. 9 (1967), p. 609.
10) R. Hill, The Mathematical Theory of Plasticity. Oxford University Press, Oxford (1950), p. 318.